Journal of Magnetic Resonance 213 (2011) 166–170

Contents lists available at SciVerse ScienceDirect

Journal of Magnetic Resonance

journal homepage: www.elsevier.com/locate/jmr

Communication

Acceleration of multi-dimensional propagator measurements with compressed sensing

Jeffrey L. Paulsen [a,**], HyungJoon Cho [b], Gyunggoo Cho [c], Yi-Qiao Song [a,*]

[a] Schlumberger-Doll Research, One Hampshire St., Cambridge MA, United States
[b] School of Nano-Bioscience and Chemical Engineering, UNIST, Ulsan, South Korea
[c] Korea Basic Science Institute, Ochang, South Korea

ARTICLE INFO

Article history:
Received 21 June 2011
Revised 10 August 2011
Available online 23 August 2011

Keywords:
NMR
Diffusion
Compressed sensing
Propagator
2D and 3D diffusion propagator

ABSTRACT

NMR can probe the microstructures of anisotropic materials such as liquid crystals, stretched polymers and biological tissues through measurement of the diffusion propagator, where internal structures are indicated by restricted diffusion. Multi-dimensional measurements can probe the microscopic anisotropy, but full sampling can then quickly become prohibitively time consuming. However, for incompletely sampled data, compressed sensing is an effective reconstruction technique to enable accelerated acquisition. We demonstrate that with a compressed sensing scheme, one can greatly reduce the sampling and the experimental time with minimal effect on the reconstruction of the diffusion propagator with an example of anisotropic diffusion. We compare full sampling down to 64× sub-sampling for the 2D propagator measurement and reduce the acquisition time for the 3D experiment by a factor of 32 from ~80 days to ~2.5 days.

1. Introduction

Measuring the directional dependence of diffusion with NMR is a useful tool to characterize the complicated internal microstructure for many anisotropic materials, such as liquid crystals [1–3], ordered polymer structures [4], stretched polymer electrolytes [5], nanostructured materials [6,7], and biological tissues [8,9] and may help further resolve the NMR spectra of such mixtures with DOSY [10,11] as well. Diffusion tensor measurements only require few independent encodings, a minimum of six along different directions, and provide only a simple model (diffusion tensor) for anisotropic diffusion. However, it is well known [12] that this model may lack the angular resolution necessary to identify more complex structures, like fiber crossings in biological networks, due to the underlying Gaussian assumption. For diffusive motion, the Gaussian approximation breaks down as the diffusion length approaches the size on any confining structures [12]. For non-biological porous media applications, such as characterizing the pore structure of rocks, this can often be the case as pore sizes can span orders of magnitude.

Variations from non-Gaussian diffusive behavior has motivated a variety of different NMR encoding and reconstruction schemes such as low q scattering experiments [13], q-ball [14] and kurtosis imaging [15]. Common to these approaches, is that they are model-dependent, relying on the highly regular structure of the diffusion propagator, fitting to a targeted basis such as spherical harmonics or performing something along the lines of a cumulant analysis [16]. However, these are not always extendable to the wider range of propagator measurements, for instance in the presence of flow [17] or in propagator–propagator exchange experiments [18]. Furthermore, in certain rare pathological systems, such as well ordered bead packs [19], resonance effects can still be observed corresponding to pore exchange that some of these newer sequences aim to produce for a wider range of materials.

Alternatively, inverting for the model, free diffusion propagator [20] yields the probability distribution $P(\Delta x, \Delta t)$ of displacement Δx of the fluid's individual molecules for one or multiple travel times Δt. Deviations from free diffusion and the shape of the propagator yields information about the microscopic structure as these restrict diffusive motion without any additional assumptions placed on the diffusion process. Multidimensional versions of these measurements, looking at the directionality of the diffusion propagator [21] are necessary to yield details of the microscopic anisotropy, and the generality of the full propagator inversion allows it to be applied to a wider variety of these experiments.

While multidimensional measurements are necessary to fully probe the anisotropy of the microstructure from the propagator, they greatly increase the sampling requirements for full reconstruction and hence experiment time. For example, a fully sampled 3D, high-resolution (e.g. 128 × 128 × 128, for 128 samples along each dimension) propagator measurement with a 3s repetition

* Corresponding author.
** Principle corresponding author.
E-mail addresses: jpaulsen2@slb.com (J.L. Paulsen), hjcho@unist.ac.kr (H. Cho), gyunggoo@kbsi.re.kr (G. Cho), ysong@slb.com (Y.-Q. Song).

1090-7807/$ - see front matter © 2011 Elsevier Inc. All rights reserved.
doi:10.1016/j.jmr.2011.08.025

time would lead to a ~80 day experiment time. The resulting long experiment times pose a major limitation to the application of multidimensional diffusion propagator techniques.

Compressed Sensing (CS), has become an effective tool in NMR and MRI for accelerating data acquisition, and it is a general method for a wide range of applications where signal processing is involved in data reconstruction [22]. Following the notational conventions presented in [23], the problem is to reconstruct some vector m, in this case describing the full diffusion propagator, from the subsampled data vector y (our signal in q-space), which are related by some linear operator F_u (the subsampled Fourier operator). However, as the collected data is subsampled, strictly speaking, there are many solutions for m that are technically consistent with the observation y. To resolve this ambiguity, CS can be described as reconstructing from subsampled data by optimizing for the reconstruction's sparsity under some predetermined linear compressive transformation, $\mathbf{\Psi}$. [22] This is achieved by minimizing the l_1-norm, defined as $\|x\|_1 = \sum_i |x_i|$, of the compressed reconstruction [23–25] that is consistent with the acquired data. In comparison, a least-squares fit or equivalently an l_2-minimization would discourage sparse solutions, as it disproportionately penalizes coefficients with large values in favor or reconstructions with their intensity spread out over multiple coefficients. Thus, in the presence of noise [26], the optimization for a CS reconstruction can be summarized as [23]:

$$\min \|\Psi m\|_1 \quad \text{s.t.} \quad \|F_u m - y\|_2 < \varepsilon.$$

As most spectra and images are compressible under some transformation, Ψ [23], for instance total variation, wavelet or curvelet, and the technique is not specific to a particular reconstruction transform (Fourier, Hadamard, etc.), CS is very general and can potentially be applied to a wide variety of detection and encoding schemes. It only requires that the transform is linear and, to describe it qualitatively, a subset of data samples can incoherently cover the reconstruction. The concept behind CS, l_1-minimization of a sparse spectra for subsampled reconstruction is well documented, for example in Donoho et al. [27], but its more recent popularity has been due to the development of the supporting theory [25,26] placing bounds on the sampling requirements (random/incoherent), sparsity and appropriate reconstruction and compression transforms which are introduced in greater detail in Candes and Wakin [22]. Its application to accelerating NMR and MRI started with its initial demonstration by Lustig et al. for MRI imaging [23]. Compressed sensing, as a general reconstruction technique, can just as well be applied to multidimensional propagator measurements with NMR. Here, CS has already been shown to be able to accurately extract angular dependence [28], but not for the larger propagator datasets necessary for high propagator resolution experiments that should furthermore allow for higher subsampling ratios [23,29].

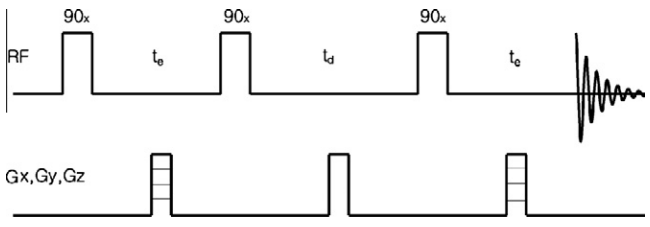

Fig. 1. The pulsed gradient stimulated echo experiment (PGSE). An initial 90° RF-pulse excites the spins and a gradient pulse encodes for position. A second 90° pulse stores the magnetization and to allow for a longer diffusion time during which a gradient pulse spoils any remaining transverse magnetization. The final 90° pulse places the magnetization back into the transverse plane to generate a stimulated echo. Here a final gradient pulse matched in length and amplitude to the first effectively decodes the position leaving only the residual encoding due to motion within the stimulated echo's signal.

Diffusion propagators are typically measured using a pair of magnetic field gradient pulses with equal but opposite amplitude separated by a time Δt (see Fig. 1) [30,31]. If the molecules do not diffuse during this time, then the effects of the gradients cancel. Any displacement of spins is encoded in this experiment as a phase proportional to the applied gradient [20]. Thus Fourier transform of the signal as a function of the gradient will determine the diffusion propagator in a fashion analogous to the Fourier encoding in NMR spectroscopy or MR imaging, except that the measurement now corresponds to displacement instead of chemical shift or position. Hence, the identical approach to sampling (random weighted towards low encoding values) and reconstruction (wavelet compression) as for CS reconstruction of images may be applied [23].

For this application, the Gaussian distribution serves to ensure a sampling bias towards small q-space values, while still collecting enough data at large ones. Biasing towards low encoding values better ensures good signal to noise, but must be balanced against maintaining sampling incoherence and the need to collect a sufficient number of the larger q-values to reconstruct the propagator's details. Even with an 'optimal' distribution, multiple random instances of it can still have a greatly varied effect [29] and the reader is referenced to [23,29] for details as to their 'optimization.' These approaches are inexact and to the author's knowledge the theoretical optimal sampling for CS where the signal is noisy and consistently biased has yet to be presented.

The other design variable for a CS implementation is the compression transform. The very regular nature of the propagator relative to most MR images, should lead to higher compression ratios for fewer sparse coefficients and hence lower sampling requirements [23,25]. Nonetheless, our selection of wavelet compression in comparison to a transform targeted to the structure of the diffusion propagator, for instance spherical harmonics, will likely offer sub-optimal compression. However, the wavelet transform has significantly greater generality and would be applicable to other types of propagator measurements for the characterization of porous media such as flow [32] or propagator correlation [18] techniques. The purpose of this study is to evaluate the ability of CS to reconstruct propagator measurements, with the simplest multidimensional type, the anisotropic diffusion propagator.

2. Results and discussion

A sample of asparagus stalk was used as a simple homogeneous anisotropic material to test the CS reconstruction of the propagator measurements. It is known that the bundles of elongated cells are aligned along the stalk and that there is significant diffusion restriction perpendicular to its axis. For this sample, a fully sampled 256×256 2D (Fig. 2) and a $32\times$ subsampled $128 \times 128 \times 128$ 3D propagator (Fig. 3) were acquired at a 2.8 μm resolution. Subsampling for the 2D propagator was obtained by reconstructing from subsets of the fully sampled 256×256 dataset. Both the full 2D and 3D acquisitions took ~2.5 days.

The 2D propagators obtained from the full 2D dataset and the subsampled datasets are shown in Fig. 2. There is significantly more diffusional displacement along the stalk (Δz) than perpendicular to its axis ($\Delta x, \Delta y$) as clearly shown by the narrowing of the propagator along the Δy-axis. This is a reflection of the homogeneous and anisotropic nature of the sample's microstructure. The cells are elongated and their walls restrict motion resulting in anisotropic diffusion with greater motion along the cell length. As the sample is macroscopically homogeneous, in that the cells are in bundles all aligned along the stalk's axis, this anisotropic motion is observed in the propagator of the bulk sample. With the subsampling of the 2D measurement, little apparent

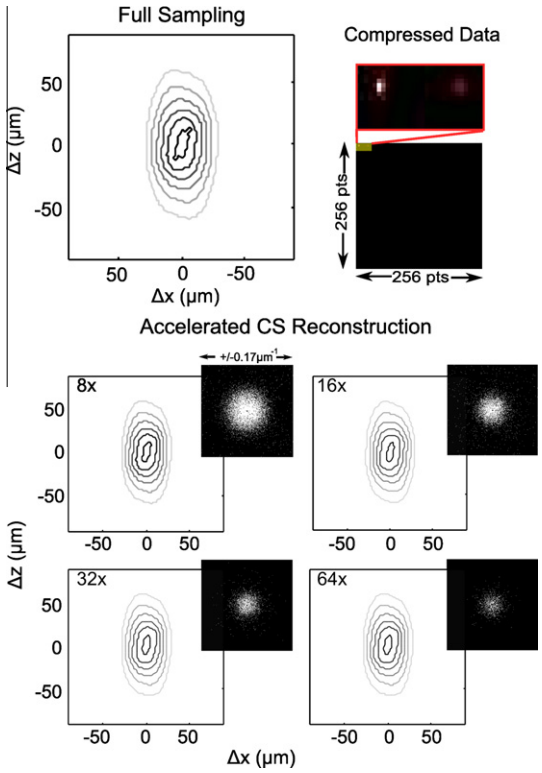

Fig. 2. The 2D propagator reconstructed from fully sampled data and with increasing degrees of subsampling (8×, 16×, 32× and 64×) with CS, shown for a quarter of the total range of displacements encoded for the the propagator, 179.2 μm (of 716.8 μm), with contours at 15%, 28%, 42%, 55%, 69%, 82%, and 96% of maximum signal. An image of the wavelet compressed reconstruction is shown adjacent to the fully sampled data. Its l_1-norm is minimized within the CS reconstruction and is sparse as required. The sub-sampling tables indicate the points in q-space (the complex Fourier transform of the propagator) that PGSE experiment would collect, and are shown adjacent to their respective reconstructions. As the sequence also relied on the gradient encoding for coherence selection, the small black dots at the plot's centers reflect the center q-space points that then had to be omitted due to inadequate gradient strength.

degradation in the reconstructed propagator occurs as seen in the reconstructions of the full to 64× subsampled data (Fig. 2). The sampling schemes, shown adjacent to the corresponding reconstructions for the 2D reconstructions, are randomly sampled with a Gaussian weighting focused on the center to approximately correspond to the expected signal distribution. While surprisingly few samples are required, the number of sparse coefficients for them to support is quite small (nearly unnoticeable) as shown in the compressed wavelet domain plotted adjacent to the fully sampled propagator in Fig. 2. Quantitatively, within the 2D reconstructions, the deviation of the propagator is within 1–4% of the peak intensity (Fig. 4), worse for the greatest degree of subsampling (64×) and most apparent along the 'x-axis', the 2nd dimension of the acquisition where spectrometer instabilities (such as imperfections in adjusting for frequency drift) would be the greatest.

The 3D propagator for the sample again shows (Fig. 3) greater diffusion along the stalk's axis (Δz) than perpendicular to it ($\Delta x, \Delta y$). As the plants cells are both elongated and uniformly aligned along the z axis and the sample is isotropic within the xy-plane, the diffusion propagator appears circular (Fig. 3) within this slice. The xz- and yz-planes of the 3D diffusion propagator (Fig. 3) are qualitatively similar to the 2D diffusion propagator (Fig. 2) and clearly show a widened distribution along the stalk's axis. However, they differ quantitatively, as the 2D propagator is a projection of this 3D dataset, integrating over the Δy-axis. For a quantitative comparison, the 3D data is projected (summed) into the xz-plane and plotted against the 2D reconstructions along the primary axes (Fig. 4). The reconstruction has systematic errors on the order of ~5% of the maximum intensity away from the fully sampled 2D propagator. Given the superior performance of 64× subsampling for the 2D propagator, these systematic errors are mostly attributable to the acquisition. With 32× subsampling, the 3D acquisition still lasts the same time as the fully sampled 2D experiment for the same degree of drift, but only obtains partial data. Acquiring at the same resolution with half the number of points per dimension furthermore results in a lower density of small gradient encoded samples, where the signal is concentrated, and both result in lower signal to noise. All of these factors would make the 3D data more sensitive to errors in the acquisition.

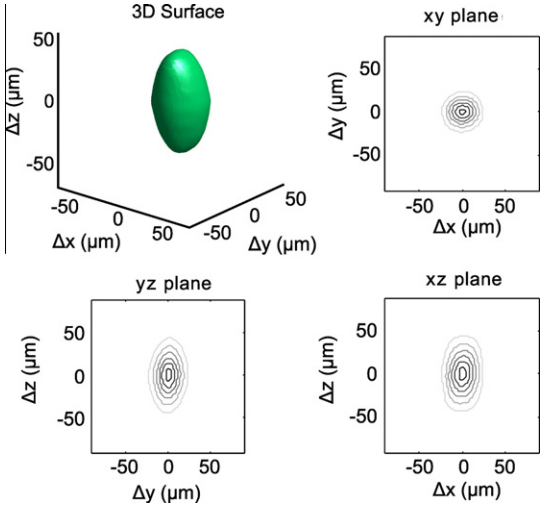

Fig. 3. CS reconstruction of the 3D diffusion propagator (128 × 128 × 128) subsampled by 32× showing preferential diffusion along the asparagus stalk (z). The surface plot (set at 33% max. signal intensity) shows the angular dependence of diffusion while the contour plots (15%, 28%, 42%, 55%, 69%, 82%, and 96% max. signal) of the center slices of the three planes detail its structure.

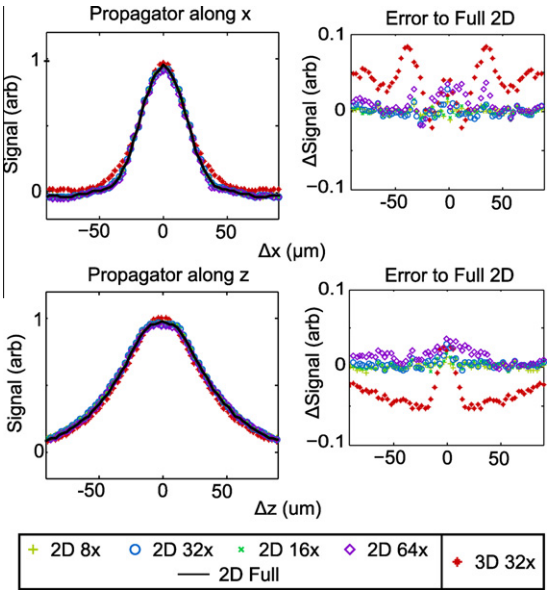

Fig. 4. The propagator (left) and the difference to the fully sampled data (right) along the lines $\Delta z = 0$ (top) and $\Delta x = 0$ (bottom). These directly compare the CS reconstructions for the 2D propagator under varying degrees of subsampling and with respect to the 3D propagator after projection onto the 2D plane.

The performance of CS is quite good for our 2D and 3D data, and even for very high subsampling ratios (64×). This is mainly due to the very simple and compressible nature of the diffusion propagator, so that it can be adequately described with very few sparse coefficients and hence requires correspondingly few samples to reconstruct [16,18,19]. However, as indicated by greater increases in error with subsampling along the slowly acquired dimension, CS reconstruction further sensitizes the results to experimental drift and imperfections in the sequence. Unlike pure random noise, the 'signal' from systematic errors can compress under transformation, but differently from the propagator, and may bias the CS reconstruction which simply optimizes for an l_1 measure of compression. Furthermore, these corruptions of the signal can reduce the sparsity of the acquired data and hence increase the number of necessary samples to accurately represent it. Nonetheless, CS was still quite effective at reconstructing the propagator given sufficient diligence to minimize and correct experimental artifacts before CS reconstruction. For their identification and mitigation, we reference the reader to Price's review on the topic [33].

3. Conclusions

This work demonstrates that Compressed Sensing (CS) allows for substantial subsampling (32× and 64×) of real experimental propagator data. As a general reconstruction technique, CS reconstruction could be applied to the wide variety of flow and propagator data lacking the structure and symmetry found in the diffusion propagator measurements that we obtained here. The disadvantage of this generality for measuring diffusion propagators in particular, is that then places far weaker priors on the reconstruction and should not necessarily have better performance than existing techniques that address the typically minor deviations from non-Gaussian behavior. Our results, though tested with a particular pulse sequence, PGSE, are general to any other implementation that yields Fourier encoding of the diffusion propagator, for instance DOSY for NMR spectroscopy, or Difftrain [34], single-scan 2D [35] and MMME [36,37] for even further accelerated measurements through the acquisition of multiple diffusion times or multiple encodings per scan. In addition to the use of other pulse sequences, further improvements in sampling and reconstruction are possible, as the compression (Wavelet) and sampling (random Gaussian) used are based from existing work on image reconstruction and have not been tailored to the diffusion propagator. For diffusion propagator measurements in particular, compression with a targeted basis such as spherical polar Fourier [28], and a sampling scheme target to its structure, further improvements in performance and reconstruction fidelity should be possible. Thus, in conjunction with careful experimental setup, our 2.5 day 3D propagator measurement may potentially be reduced to hours. Similarly, flow and correlation propagator experiments should be able to experience similar acceleration factors.

4. Experimental

The propagator was measured using a standard pulsed field gradient stimulated echo experiment (PGSE) sequence [13] on a Bruker 600 MHz vertical narrow bore spectrometer with a 100 G/cm gradient system and a Helmholtz RF coil (2.8 cm long, 1 cm inner diameter). A stimulated echo experiment was selected so to maximize the available diffusion time by making T_1 instead of T_2 or T_2^* as its limiting factor. The sequence was implemented with 26 μs RF excitation and refocusing pulses and two separate 8 ms long encoding gradient pulses incremented together with identical amplitudes up to a maximum of 51.2 G/cm and separated by a 460 ms delay. For both the fully sampled two-dimensional and sub-sampled three-dimensional propagator measurements 65,536 (256×256 and 32× subsampled $128 \times 128 \times 128$) independent q-space encodings were collected both at a 2.8 μm propagator resolution for 716.8 μm and 358.4 μm ranges of resolved displacements respectively.

The sampling tables were randomly generated with a Gaussian weighting as detailed in prior work [29] and discussed previously in the introduction. Instead of phase-cycling, the sequence only collected a single scan and used the encoding magnetic field gradients for coherence selection in addition to encoding, so the omission of data from very low-gradient amplitude samples was necessary to avoid signal arising from T_1 relaxation during the diffusion time. Since only a small number of adjacent points at the center of q-space were removed, this did not significantly affect the 'incoherence' of the sampling, nor was the available signal significantly reduced since the vast majority of small q-space components were still retained. However, greatly enlarging this omitted region would ruin the signal-to-noise, and, because of a loss of sampling 'incoherence', make it difficult for CS to resolve 'low frequency' structures generating baseline like errors [29].

Before CS reconstruction, the complex echo amplitudes were extracted by integration of the water peak after Fourier transformation of the collected time domain signal apodized by an exponential decay. Due to spectrometer frequency drift and a lack of a deuterium lock signal, the frequency drift was adjusted in post-processing by moving the center of the integration window according to the 1st moment of the absolute value spectrum of the nearest sample in experiment time with sufficient SNR to accurately determine peak position. The CS reconstruction, consisting of the constrained l_1-minimization stated in the introduction, was implemented in Matlab incorporating the libraries spgl1 [38] for the l_1-optimizer and Wavelab [39] for the fast wavelet transform for compression and originates from prior work [29]. The noise level, ε, for the reconstruction was set to a fraction of the estimated noise, obtained from the signal of a subset of strong gradient encoded points after subtracting the 1st order polynomial fit of their values.

Acknowledgments

H. Cho acknowledges the receipt of the National Research Foundation of Korea Grants funded by the Korean Government (No. 2010-0029434 and No. 2010-0003608).

References

[1] P.T. Callaghan, S. Godefroy, B.N. Ryland, Use of the second dimension in PGSE NMR studies of porous media, Magnetic Resonance Imaging 21 (3) (2003) 243–248.
[2] S.V. Dvinskikh, I. Furó, Nuclear magnetic resonance studies of translational diffusion in thermotropic liquid crystals, Russian Chemical Reviews 75 (6) (2006) 497–506.
[3] P.L. Hubbard, K.M. McGrath, P.T. Callaghan, Orientational Anisotropy in the Polydomain Lamellar Phase of a Lyotropic Liquid Crystal, Langmuir 22 (9) (2006) 3999–4003.
[4] F. Rittig, G. Fleischer, J. Kärger, C.M. Papadakis, K. Almdal, P. Štěpánek, Anisotropic self-diffusion in a hexagonally ordered asymmetric PEP−PDMS diblock copolymer studied by pulsed field gradient NMR, Macromolecules 32 (18) (1999) 5872–5877.
[5] D. Golodnitsky et al., Fast ion transport phenomena in oriented semicrystalline LiI−P(EO)n-based polymer electrolytes, The Journal of Physical Chemistry A 105 (44) (2001) 10098–10106.
[6] S. Naumov, R. Valiullin, J. Kärger, R. Pitchumani, M.-O. Coppens, Tracing pore connectivity and architecture in nanostructured silica SBA-15, Microporous and Mesoporous Materials 110 (1) (2008) 37–40.
[7] J. Kärger et al., Benefit of microscopic diffusion measurement for the characterization of nanoporous materials, Chemical Engineering & Technology 32 (10) (2009) 1494–1511.
[8] P.J. Basser, J. Mattiello, D. Lebihan, Estimation of the effective self-diffusion tensor from the NMR Spin Echo, Journal of Magnetic Resonance, Series B 103 (3) (1994) 247–254.

[9] P.J. Basser, D.K. Jones, Diffusion-tensor MRI: theory, experimental design and data analysis – a technical review, NMR in Biomedicine 15 (7-8) (2002) 456–467.
[10] B. Antalek, W. Windig, Generalized rank annihilation method applied to a single multicomponent pulsed gradient Spin Echo NMR data set, Journal of the American Chemical Society 118 (42) (1996) 10331–10332.
[11] T. Megyes et al., X-ray diffraction and DOSY NMR characterization of self-assembled supramolecular metallocyclic species in solution, Journal of the American Chemical Society 127 (30) (2005) 10731–10738.
[12] D.S. Grebenkov, Use, misuse, and abuse of apparent diffusion coefficients, Concepts in Magnetic Resonance Part A 36 (1) (2010) 24–35.
[13] Y. Cheng, D.G. Cory, Multiple scattering by NMR, Journal of the American Chemical Society 121 (34) (1999) 935–7936.
[14] D.S. Tuch, Q-ball imaging, Magnetic Resonance in Medicine 52 (6) (2004) 1358–1372.
[15] H. Lu, J.H. Jensen, A. Ramani, J.A. Helpern, Three-dimensional characterization of non-gaussian water diffusion in humans using diffusion kurtosis imaging, NMR in Biomedicine 19 (2) (2006) 236–247.
[16] C. Liu, R. Bammer, M.E. Moseley, Limitations of apparent diffusion coefficient-based models in characterizing non-gaussian diffusion, Magnetic Resonance in Medicine 54 (2) (2005) 419–428.
[17] U.M. Scheven, J.P. Crawshaw, V.J. Anderson, R. Harris, M.L. Johns, L.F. Gladden, A cumulant analysis for non-Gaussian displacement distributions in Newtonian and non-Newtonian flows through porous media, Magnetic Resonance Imaging 25 (4) (2007) 513–516.
[18] N. Shemesh, E. Özarslan, P.J. Basser, Y. Cohen, Measuring small compartmental dimensions with low-*q* angular double-PGSE NMR: The effect of experimental parameters on signal decay, Journal of Magnetic Resonance 198 (1) (2009) 15–23.
[19] J.D. Seymour, P.T. Callaghan, Flow-diffraction' structural characterization and measurement of hydrodynamic dispersion in porous media by PGSE NMR, Journal of Magnetic Resonance, Series A 122 (1) (1996) 90–93.
[20] Paul T. Callaghan, Principles of Nuclear Magnetic Resonance Microscopy, Clarendon Press, 1991.
[21] M.I. Menzel, S.-I. Han, S. Stapf, B. Blümich, NMR characterization of the pore structure and anisotropic self-diffusion in salt water ice, Journal of Magnetic Resonance 143 (2) (2000) 376–381.
[22] E.J. Candes, M.B. Wakin, An introduction to compressive sampling, Signal Processing Magazine IEEE 25 (2) (2008) 21–30.
[23] M. Lustig, D. Donoho, J.M. Pauly, Sparse MRI: the application of compressed sensing for rapid MR imaging, Magnetic Resonance in Medicine 58 (6) (2007) 1182–1195.
[24] J. Romberg, Imaging via compressive sampling, Signal Processing Magazine, IEEE 25 (2) (2008) 14–20.
[25] D.L. Donoho, Compressed sensing, IEEE Transactions on Information Theory 52 (4) (2006) 1289–1306.
[26] E.J. Candès, J.K. Romberg, T. Tao, Stable signal recovery from incomplete and inaccurate measurements, Communications on Pure and Applied Mathematics 59 (8) (2006) 1207–1223.
[27] D.L. Donoho, Iain M. Johnstone, J.C. Hoch, A.S. Stern, Maximum entropy and the nearly black object, Journal of the Royal Statistical Society, Series B 54 (1) (1992) 41–81.
[28] S. Merlet, J. Cheng, A. Ghosh, R. Deriche, Spherical polar Fourier EAP and ODF reconstruction via compressed sensing in diffusion MRI, ISBI (2011).
[29] J. Paulsen, V.S. Bajaj, A. Pines, Compressed sensing of remotely detected MRI velocimetry in microfluidics, Journal of Magnetic Resonance 205 (2) (2010) 196–201.
[30] J.E. Tanner, Restricted self-diffusion of protons in colloidal systems by the pulsed-gradient, Spin-Echo method, The Journal of Chemical Physics 49 (4) (1968) 1768.
[31] E.O. Stejskal, J.E. Tanner, Spin diffusion measurements: Spin Echoes in the presence of a time-dependent field gradient, The Journal of Chemical Physics 42 (1) (1965) 288.
[32] D. Verganelakis et al., Displacement propagators of brine flowing within different types of sedimentary rock, Magnetic Resonance Imaging 23 (2) (2005) 349–351.
[33] W.S. Price, Pulsed-field gradient nuclear magnetic resonance as a tool for studying translational diffusion: Part II. Experimental aspects, Concepts in Magnetic Resonance 10 (4) (1998) 197–237.
[34] J.P. Stamps, B. Ottink, J.M. Visser, J.P.M. van Duynhoven, R. Hulst, Difftrain: a novel approach to a true spectroscopic single-scan diffusion measurement, Journal of Magnetic Resonance 151 (1) (2001) 28–31.
[35] Y. Shrot, L. Frydman, Single-scan 2D DOSY NMR spectroscopy, Journal of Magnetic Resonance 195 (2) (2008) 226–231.
[36] E.E. Sigmund, Y.-Q. Song, Multiple echo diffusion tensor acquisition technique, Magnetic resonance imaging 24 (1) (2006) 7–18.
[37] Y.-Q. Song, X. Tang, A one-shot method for measurement of diffusion, Journal of Magnetic Resonance 170 (1) (2004) 136–148.
[38] E. van den Berg, M.P. Friedlander, Probing the Pareto Frontier for basis Pursuit solutions, SIAM Journal on Scientific Computing 31 (2) (2009) 890.
[39] O. Rioul, M. Vetterli, Wavelets and signal processing, Signal Processing Magazine, IEEE 8 (4) (1991) 14–38.